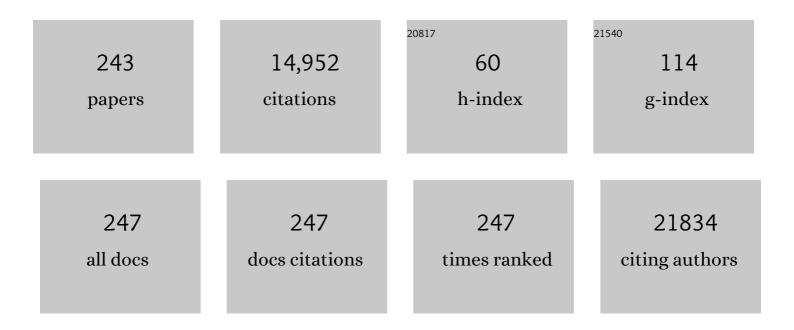
List of Publications by Year in descending order

Source: https://exaly.com/author-pdf/7558331/publications.pdf Version: 2024-02-01



DENC WANC

#	Article	IF	CITATIONS
1	Free-standing graphene at atomic resolution. Nature Nanotechnology, 2008, 3, 676-681.	31.5	575
2	High-resolution detection of Au catalyst atoms in Si nanowires. Nature Nanotechnology, 2008, 3, 168-173.	31.5	575
3	Robust memristors based on layered two-dimensional materials. Nature Electronics, 2018, 1, 130-136.	26.0	539
4	Surface-Enhanced Raman Scattering Active Gold Nanoparticles with Enzyme-Mimicking Activities for Measuring Glucose and Lactate in Living Tissues. ACS Nano, 2017, 11, 5558-5566.	14.6	514
5	Interlayer Transition and Infrared Photodetection in Atomically Thin Type-II MoTe <sub>2</sub> /MoS <sub>2</sub> van der Waals Heterostructures. ACS Nano, 2016, 10, 3852-3858.	14.6	453
6	Room temperature high-detectivity mid-infrared photodetectors based on black arsenic phosphorus. Science Advances, 2017, 3, e1700589.	10.3	419
7	Freestanding crystalline oxide perovskites down to the monolayer limit. Nature, 2019, 570, 87-90.	27.8	398
8	Epitaxial growth of wafer-scale molybdenum disulfide semiconductor single crystals on sapphire. Nature Nanotechnology, 2021, 16, 1201-1207.	31.5	339
9	Nitrogenâ€Ðoped CoP Electrocatalysts for Coupled Hydrogen Evolution and Sulfur Generation with Low Energy Consumption. Advanced Materials, 2018, 30, e1800140.	21.0	336
10	Broadband Photovoltaic Detectors Based on an Atomically Thin Heterostructure. Nano Letters, 2016, 16, 2254-2259.	9.1	322
11	Controlled Synthesis of Lead-Free and Stable Perovskite Derivative Cs <sub>2</sub> SnI <sub>6</sub> Nanocrystals via a Facile Hot-Injection Process. Chemistry of Materials, 2016, 28, 8132-8140.	6.7	310
12	Towards efficient solar hydrogen production by intercalated carbon nitride photocatalyst. Physical Chemistry Chemical Physics, 2013, 15, 18077.	2.8	309
13	Electrocatalytic Hydrogen Evolution Reaction on Edges of a Few Layer Molybdenum Disulfide Nanodots. ACS Applied Materials & Interfaces, 2015, 7, 14113-14122.	8.0	295
14	Compact Plasmonic Blackbody for Cancer Theranosis in the Near-Infrared II Window. ACS Nano, 2018, 12, 2643-2651.	14.6	294
15	Lithiation-induced amorphization of Pd3P2S8 for highly efficient hydrogen evolution. Nature Catalysis, 2018, 1, 460-468.	34.4	247
16	Strain Dynamics of Ultrathin VO <sub>2</sub> Film Grown on TiO <sub>2</sub> (001) and the Associated Phase Transition Modulation. Nano Letters, 2014, 14, 4036-4043.	9.1	233
17	Stable iridium dinuclear heterogeneous catalysts supported on metal-oxide substrate for solar water oxidation. Proceedings of the National Academy of Sciences of the United States of America, 2018, 115, 2902-2907.	7.1	229
18	Probing Carrier Transport and Structure-Property Relationship of Highly Ordered Organic Semiconductors at the Two-Dimensional Limit. Physical Review Letters, 2016, 116, 016602.	7.8	220

#	Article	IF	CITATIONS
19	The simplest construction of single-site catalysts by the synergism of micropore trapping and nitrogen anchoring. Nature Communications, 2019, 10, 1657.	12.8	220
20	Highâ€Mobility Multilayered MoS <sub>2</sub> Flakes with Low Contact Resistance Grown by Chemical Vapor Deposition. Advanced Materials, 2017, 29, 1604540.	21.0	214
21	Uniform and ultrathin high-l <sup>°</sup> gate dielectrics for two-dimensional electronic devices. Nature Electronics, 2019, 2, 563-571.	26.0	204
22	eg occupancy as an effective descriptor for the catalytic activity of perovskite oxide-based peroxidase mimics. Nature Communications, 2019, 10, 704.	12.8	199
23	Highly sensitive visible to infrared MoTe <sub>2</sub> photodetectors enhanced by the photogating effect. Nanotechnology, 2016, 27, 445201.	2.6	188
24	Uniform nucleation and epitaxy of bilayer molybdenum disulfide on sapphire. Nature, 2022, 605, 69-75.	27.8	174
25	Platinum Integrated Graphene for Methanol Fuel Cells. Journal of Physical Chemistry C, 2010, 114, 15837-15841.	3.1	163
26	Synthesis of synergetic phosphorus and cyano groups ( C N) modified g-C3N4 for enhanced photocatalytic H2 production and CO2 reduction under visible light irradiation. Applied Catalysis B: Environmental, 2018, 232, 521-530.	20.2	162
27	Ultrasonic activation of inert poly(tetrafluoroethylene) enables piezocatalytic generation of reactive oxygen species. Nature Communications, 2021, 12, 3508.	12.8	153
28	Surface Structural Transition Induced by Gradient Polyanionâ€Doping in Liâ€Rich Layered Oxides: Implications for Enhanced Electrochemical Performance. Advanced Functional Materials, 2016, 26, 4760-4767.	14.9	151
29	Nanoporous Zn-doped Co3O4 sheets with single-unit-cell-wide lateral surfaces for efficient oxygen evolution and water splitting. Nano Energy, 2018, 44, 371-377.	16.0	138
30	Epitaxial Ultrathin Organic Crystals on Graphene for Highâ€Efficiency Phototransistors. Advanced Materials, 2016, 28, 5200-5205.	21.0	134
31	Magnetic Semiconductor Gd-Doping CuS Nanoparticles as Activatable Nanoprobes for Bimodal Imaging and Targeted Photothermal Therapy of Gastric Tumors. Nano Letters, 2019, 19, 937-947.	9.1	132
32	Ruthenium–platinum core–shell nanocatalysts with substantially enhanced activity and durability towards methanol oxidation. Nano Energy, 2016, 21, 247-257.	16.0	121
33	Self-Assembled Growth, Microstructure, and Field-Emission High-Performance of Ultrathin Diamond Nanorods. ACS Nano, 2009, 3, 1032-1038.	14.6	119
34	Manganeseâ€Based Naâ€Rich Materials Boost Anionic Redox in Highâ€Performance Layered Cathodes for Sodiumâ€Ion Batteries. Advanced Materials, 2019, 31, e1807770.	21.0	113
35	Dandelion-like Mn/Ni Co-doped CoO/C Hollow Microspheres with Oxygen Vacancies for Advanced Lithium Storage. ACS Nano, 2019, 13, 11921-11934.	14.6	106
36	Ferroelectricity in untwisted heterobilayers of transition metal dichalcogenides. Science, 2022, 376, 973-978.	12.6	105

#	Article	IF	CITATIONS
37	Engineering hetero-epitaxial nanostructures with aligned Li-ion channels in Li-rich layered oxides for high-performance cathode application. Nano Energy, 2017, 35, 271-280.	16.0	99
38	Biological Uptake, Distribution, and Depuration of Radio-Labeled Graphene in Adult Zebrafish: Effects of Graphene Size and Natural Organic Matter. ACS Nano, 2017, 11, 2872-2885.	14.6	98
39	Achieving high thermoelectric performance with Pb and Zn codoped polycrystalline SnSe via phase separation and nanostructuring strategies. Nano Energy, 2018, 53, 683-689.	16.0	98
40	Stacking-mode confined growth of 2H-MoTe2/MoS2 bilayer heterostructures for UV–vis–IR photodetectors. Nano Energy, 2018, 49, 200-208.	16.0	96
41	Twoâ€Dimensional Semiconductors Grown by Chemical Vapor Transport. Angewandte Chemie - International Edition, 2017, 56, 3611-3615.	13.8	92
42	Surface Engineering of CoMoS Nanosulfide for Hydrodeoxygenation of Lignin-Derived Phenols to Arenes. ACS Catalysis, 2019, 9, 259-268.	11.2	90
43	Experimental realization of two-dimensional artificial skyrmion crystals at room temperature. Physical Review B, 2014, 90, .	3.2	89
44	Electron ptychographic microscopy for three-dimensional imaging. Nature Communications, 2017, 8, 163.	12.8	89
45	Atomic interpretation of high activity on transition metal and nitrogen-doped carbon nanofibers for catalyzing oxygen reduction. Journal of Materials Chemistry A, 2017, 5, 3336-3345.	10.3	88
46	Enhanced Water‧plitting Performance of Perovskite SrTaO <sub>2</sub> N Photoanode Film through Ameliorating Interparticle Charge Transport. Advanced Functional Materials, 2016, 26, 7156-7163.	14.9	86
47	Tuning the Catalytic Activity of Graphene Nanosheets for Oxygen Reduction Reaction via Size and Thickness Reduction. ACS Applied Materials & Interfaces, 2014, 6, 19726-19736.	8.0	83
48	Gate-Induced Interfacial Superconductivity in 1T-SnSe <sub>2</sub> . Nano Letters, 2018, 18, 1410-1415.	9.1	81
49	High-density switchable skyrmion-like polar nanodomains integrated on silicon. Nature, 2022, 603, 63-67.	27.8	79
50	Enhancing the Structural Stability of Ni-Rich Layered Oxide Cathodes with a Preformed Zr-Concentrated Defective Nanolayer. ACS Applied Materials & Interfaces, 2018, 10, 39599-39607.	8.0	78
51	Heteroepitaxial oxygen-buffering interface enables a highly stable cobalt-free Li-rich layered oxide cathode. Nano Energy, 2020, 75, 104995.	16.0	74
52	Surface passivation of mixed-halide perovskite CsPb(Br <sub>x</sub> I <sub>1â^'x</sub> ) <sub>3</sub> nanocrystals by selective etching for improved stability. Nanoscale, 2017, 9, 7391-7396.	5.6	73
53	Low-dose phase retrieval of biological specimens using cryo-electron ptychography. Nature Communications, 2020, 11, 2773.	12.8	72
54	Tuning strain effect and surface composition in PdAu hollow nanospheres as highly efficient ORR electrocatalysts and SERS substrates. Applied Catalysis B: Environmental, 2020, 262, 118298.	20.2	70

#	Article	IF	CITATIONS
55	Layer-Dependent Chemically Induced Phase Transition of Two-Dimensional MoS <sub>2</sub> . Nano Letters, 2018, 18, 3435-3440.	9.1	69
56	Hierarchical sulfur and nitrogen co-doped carbon nanocages as efficient bifunctional oxygen electrocatalysts for rechargeable Zn-air battery. Journal of Energy Chemistry, 2019, 34, 64-71.	12.9	69
57	Hollow Palladiumâ€Gold Nanochains with Periodic Concave Structures as Superior ORR Electrocatalysts and Highly Efficient SERS Substrates. Advanced Energy Materials, 2020, 10, 1904072.	19.5	69
58	Achieving high structure and voltage stability in cobalt-free Li-rich layered oxide cathodes via selective dual-cation doping. Energy Storage Materials, 2020, 32, 37-45.	18.0	69
59	The Effect of Boron Doping on Structure and Electrochemical Performance of Lithium-Rich Layered Oxide Materials. ACS Applied Materials & Interfaces, 2016, 8, 18008-18017.	8.0	68
60	Constrained growth of ultrasmall BiOCl nanodiscs with a low percentage of exposed {001} facets and their enhanced photoreactivity under visible light irradiation. Applied Catalysis B: Environmental, 2015, 176-177, 201-211.	20.2	65
61	Polarized Optoelectronics of CsPbX <sub>3</sub> (X = Cl, Br, I) Perovskite Nanoplates with Tunable Size and Thickness. Advanced Functional Materials, 2018, 28, 1800283.	14.9	63
62	Electroplating lithium transition metal oxides. Science Advances, 2017, 3, e1602427.	10.3	62
63	Mechanism of Alkali Metal Compound-Promoted Growth of Monolayer MoS <sub>2</sub> : Eutectic Intermediates. Chemistry of Materials, 2019, 31, 873-880.	6.7	59
64	Strong optical response and light emission from a monolayer molecular crystal. Nature Communications, 2019, 10, 5589.	12.8	59
65	A phase-transition-free cathode for sodium-ion batteries with ultralong cycle life. Nano Energy, 2018, 52, 88-94.	16.0	58
66	Solvothermal Synthesis of Lateral Heterojunction Sb <sub>2</sub> Te <sub>3</sub> /Bi <sub>2</sub> Te <sub>3</sub> Nanoplates. Nano Letters, 2015, 15, 5905-5911.	9.1	56
67	Rational design of electrocatalysts for simultaneously promoting bulk charge separation and surface charge transfer in solar water splitting photoelectrodes. Journal of Materials Chemistry A, 2018, 6, 2568-2576.	10.3	56
68	Stable heteroepitaxial interface of Li-rich layered oxide cathodes with enhanced lithium storage. Energy Storage Materials, 2019, 21, 69-76.	18.0	53
69	Unlocking the potential of graphene for water oxidation using an orbital hybridization strategy. Energy and Environmental Science, 2018, 11, 407-416.	30.8	52
70	Boosting the performance of single-atom catalysts via external electric field polarization. Nature Communications, 2022, 13, .	12.8	52
71	Mesoporous Ce-Ti-Zr ternary oxide millispheres for efficient catalytic ozonation in bubble column. Chemical Engineering Journal, 2018, 338, 261-270.	12.7	51
72	A Superlatticeâ€Stabilized Layered Oxide Cathode for Sodiumâ€Ion Batteries. Advanced Materials, 2020, 32, e1907936.	21.0	50

#	Article	IF	CITATIONS
73	Phase transformations in yttrium –aluminium oxides in friction stir welded and recrystallised PM2000 alloys. Materials at High Temperatures, 2009, 26, 299-303.	1.0	47
74	Core–Shell Layered Oxide Cathode for High-Performance Sodium-Ion Batteries. ACS Applied Materials & Interfaces, 2020, 12, 7144-7152.	8.0	47
75	Giant Ferroelectric Polarization in Ultrathin Ferroelectrics via Boundary ondition Engineering. Advanced Materials, 2017, 29, 1701475.	21.0	47
76	Anchoring Copper Single Atoms on Porous Boron Nitride Nanofiber to Boost Selective Reduction of Nitroaromatics. ACS Nano, 2022, 16, 4152-4161.	14.6	47
77	Nanoscale Energy-Filtered Scanning Confocal Electron Microscopy Using a Double-Aberration-Corrected Transmission Electron Microscope. Physical Review Letters, 2010, 104, 200801.	7.8	46
78	Deterministic electron ptychography at atomic resolution. Physical Review B, 2014, 89, .	3.2	46
79	Fabrication of highly emissive and highly stable perovskite nanocrystal-polymer slabs for luminescent solar concentrators. Journal of Materials Chemistry A, 2019, 7, 4872-4880.	10.3	45
80	Physicochemical Changes of Few-Layer Graphene in Peroxidase-Catalyzed Reactions: Characterization and Potential Ecological Effects. Environmental Science & Technology, 2015, 49, 8558-8565.	10.0	44
81	Atomic Resolution Defocused Electron Ptychography at Low Dose with a Fast, Direct Electron Detector. Scientific Reports, 2019, 9, 3919.	3.3	44
82	Unusual Stacking Variations in Liquid-Phase Exfoliated Transition Metal Dichalcogenides. ACS Nano, 2014, 8, 3690-3699.	14.6	43
83	Study of Microstructure Change of Carbon Nanofibers as Binder-Free Anode for High-Performance Lithium-Ion Batteries. ACS Applied Materials & Interfaces, 2016, 8, 33091-33101.	8.0	43
84	Aberration measurement using the Ronchigram contrast transfer function. Ultramicroscopy, 2010, 110, 891-898.	1.9	42
85	Carbon Quantum Dots Modulated NiMoP Hollow Nanopetals as Efficient Electrocatalysts for Hydrogen Evolution. Industrial & Engineering Chemistry Research, 2019, 58, 14098-14105.	3.7	42
86	Contrast Reversal in Atomic-Resolution Chemical Mapping. Physical Review Letters, 2008, 101, 236102.	7.8	41
87	Understanding the Enhanced Kinetics of Gradient-Chemical-Doped Lithium-Rich Cathode Material. ACS Applied Materials & Interfaces, 2017, 9, 20519-20526.	8.0	41
88	Capturing Reversible Cation Migration in Layered Structure Materials for Naâ€lon Batteries. Advanced Energy Materials, 2019, 9, 1900189.	19.5	41
89	Magnetic interactions in BiFe0.5Mn0.5O3 films and BiFeO3/BiMnO3 superlattices. Scientific Reports, 2015, 5, 9093.	3.3	40
90	Direct measurement of composition of buried quantum dots using aberration-corrected scanning transmission electron microscopy. Applied Physics Letters, 2006, 89, 072111.	3.3	38

#	Article	IF	CITATIONS
91	Engineering Nanoceria for Enhanced Peroxidase Mimics: A Solid Solution Strategy. ChemCatChem, 2019, 11, 737-743.	3.7	38
92	DNA origami single crystals with Wulff shapes. Nature Communications, 2021, 12, 3011.	12.8	38
93	Electron Ptychographic Diffractive Imaging of Boron Atoms in LaB6 Crystals. Scientific Reports, 2017, 7, 2857.	3.3	37
94	Atomically Resolved Electrically Active Intragrain Interfaces in Perovskite Semiconductors. Journal of the American Chemical Society, 2022, 144, 1910-1920.	13.7	37
95	Site Occupancy and Dielectric Characteristics of Strontium Barium Niobate Ceramics: Sr/Ba Ratio Dependence. Japanese Journal of Applied Physics, 2002, 41, 7042-7047.	1.5	36
96	Repairing atomic vacancies in single-layer MoSe2 field-effect transistor and its defect dynamics. Npj Quantum Materials, 2017, 2, .	5.2	36
97	Tailoring alternating heteroepitaxial nanostructures in Na-ion layered oxide cathodes via an in-situ composition modulation route. Nano Energy, 2018, 44, 336-344.	16.0	36
98	Co-catalysis of a bi-functional ligand containing phosphine and Lewis acidic phosphonium for hydroformylation–acetalization of olefins. Green Chemistry, 2016, 18, 1798-1806.	9.0	35
99	Antiferromagnetic Order in Epitaxial FeSe Films on <mml:math xmlns:mml="http://www.w3.org/1998/Math/MathML" display="inline"&gt;<mml:mrow><mml:msub><mml:mrow><mml:mi>SrTiO</mml:mi></mml:mrow><mml:mrow><m Physical Review Letters, 2018, 120, 097001.</m </mml:mrow></mml:msub></mml:mrow></mml:math 	1718 111:mn>3	<
100	Strengthening nitrogen affinity on CuAu@Cu core–shell nanoparticles with ultrathin Cu skin via strain engineering and ligand effect for boosting nitrogen reduction reaction. Applied Catalysis B: Environmental, 2021, 288, 119999.	20.2	35
101	Tuning the transport behavior of centimeter-scale WTe2 ultrathin films fabricated by pulsed laser deposition. Applied Physics Letters, 2017, 111, .	3.3	34
102	Probing the light harvesting and charge rectification of bismuth nanoparticles behind the promoted photoreactivity onto Bi/BiOCl catalyst by (in-situ) electron microscopy. Applied Catalysis B: Environmental, 2017, 201, 495-502.	20.2	34
103	Reducing Contact Resistance and Boosting Device Performance of Monolayer MoS <sub>2</sub> by In Situ Fe Doping. Advanced Materials, 2022, 34, e2200885.	21.0	34
104	Electrical conduction mechanisms and effect of atmosphere annealing on the electrical properties of BiFeO3-BaTiO3 ceramics. Journal of the European Ceramic Society, 2019, 39, 4727-4734.	5.7	33
105	Shear-resistant interface of layered oxide cathodes for sodium ion batteries. Energy Storage Materials, 2022, 45, 389-398.	18.0	33
106	Roles of Coherent Interfaces on Electrochemical Performance of Sodium Layered Oxide Cathodes. Chemistry of Materials, 2018, 30, 4728-4737.	6.7	32
107	Revealing the Critical Role of Titanium in Layered Manganeseâ€Based Oxides toward Advanced Sodiumâ€lon Batteries via a Combined Experimental and Theoretical Study. Small Methods, 2019, 3, 1800183.	8.6	32
108	Towards rational design of high performance Ni-rich layered oxide cathodes: The interplay of borate-doping and excess lithium. Journal of Power Sources, 2019, 431, 40-47.	7.8	31

PENG WANG

#	Article	IF	CITATIONS
109	Aliovalent fluorine doping and anodization-induced amorphization enable bifunctional catalysts for efficient water splitting. Journal of Materials Chemistry A, 2020, 8, 10831-10838.	10.3	31
110	Reviving reversible anion redox in 3d-transition-metal Li rich oxides by introducing surface defects. Nano Energy, 2020, 71, 104644.	16.0	31
111	Gate-tunable the interface properties of GaAs–WSe2 (1D–2D) vdWs heterojunction for high-responsivity, self-powered photodetector. Applied Physics Letters, 2021, 118, .	3.3	31
112	Bifunctional ligands in combination with phosphines and Lewis acidic phospheniums for the carbonylative Sonogashira reaction. Chemical Communications, 2015, 51, 10871-10874.	4.1	29
113	Structural and Magnetic Characterization of Co and Ni Silicate Hydroxides in Bulk and in Nanostructures within Silica Aerogels. Chemistry of Materials, 2009, 21, 945-953.	6.7	28
114	Iron oxide nanoparticles confined in mesoporous silicates for arsenic sequestration: effect of the host pore structure. Environmental Science: Nano, 2017, 4, 679-688.	4.3	28
115	Ferrous sulfide-assisted hollow carbon spheres as sulfur host for advanced lithium-sulfur batteries. Chemical Engineering Journal, 2017, 326, 1040-1047.	12.7	28
116	Insights into the growth of bismuth nanoparticles on 2D structured BiOCl photocatalysts: an in situ TEM investigation. Dalton Transactions, 2015, 44, 15888-15896.	3.3	27
117	Direct Demonstration of the Emergent Magnetism Resulting from the Multivalence Mn in a LaMnO <sub>3</sub> Epitaxial Thin Film System. Advanced Electronic Materials, 2018, 4, 1800055.	5.1	27
118	Hollow Electron Ptychographic Diffractive Imaging. Physical Review Letters, 2018, 121, 146101.	7.8	27
119	SbSI Nanocrystals: An Excellent Visible Light Photocatalyst with Efficient Generation of Singlet Oxygen. ACS Sustainable Chemistry and Engineering, 2018, 6, 12166-12175.	6.7	27
120	Atomic Characterization of Byproduct Nanoparticles on Cesium Lead Halide Nanocrystals Using High-Resolution Scanning Transmission Electron Microscopy. Crystals, 2018, 8, 2.	2.2	27
121	Electrochemical and Structural Analysis in Allâ€Solidâ€State Lithium Batteries by Analytical Electron Microscopy: Progress and Perspectives. Advanced Materials, 2020, 32, e1903747.	21.0	27
122	Insights into the Enhanced Structural and Thermal Stabilities of Nb-Substituted Lithium-Rich Layered Oxide Cathodes. ACS Applied Materials & Interfaces, 2021, 13, 45619-45629.	8.0	26
123	Strain engineering by atomic lattice locking in P2-type layered oxide cathode for high-voltage sodium-ion batteries. Nano Energy, 2020, 76, 105061.	16.0	25
124	Programmable Assembly of Nanoâ€architectures through Designing Anisotropic DNA Origami Patches. Angewandte Chemie - International Edition, 2020, 59, 6389-6396.	13.8	25
125	Synthesis of hierarchical and bridging carbon-coated LiMn 0.9 Fe 0.1 PO 4 nanostructure as cathode material with improved performance for lithium ion battery. Journal of Power Sources, 2017, 359, 408-414.	7.8	25
126	Highly crystalline ReSe <sub>2</sub> atomic layers synthesized by chemical vapor transport. InformaÄnÃ- Materiály, 2019, 1, 552-558.	17.3	24

PENG WANG

#	Article	IF	CITATIONS
127	Geometric aspects of lattice contrast visibility in nanocrystalline materials using HAADF STEM. Ultramicroscopy, 2006, 106, 277-283.	1.9	23
128	Highly Durable and Active Ternary Pt–Au–Ni Electrocatalyst for Oxygen Reduction Reaction. ChemCatChem, 2018, 10, 3049-3056.	3.7	22
129	A Flexible Film toward Highâ€Performance Lithium Storage: Designing Nanosheetâ€Assembled Hollow Singleâ€Hole Ni–Co–Mn–O Spheres with Oxygen Vacancy Embedded in 3D Carbon Nanotube/Graphene Network. Small, 2019, 15, e1901343.	10.0	22
130	Optimization of oxygen vacancy concentration in HfO2/HfOx bilayer-structured ultrathin memristors by atomic layer deposition and their biological synaptic behavior. Journal of Materials Chemistry C, 2020, 8, 12478-12484.	5.5	22
131	Epitaxial optimization of atomically smooth Sr3Al2O6 for freestanding perovskite films by molecular beam epitaxy. Thin Solid Films, 2020, 697, 137815.	1.8	22
132	Optical Sectioning and Confocal Imaging and Analysis in the Transmission Electron Microscope. Annual Review of Materials Research, 2012, 42, 125-143.	9.3	21
133	Effect of positive-charges in diphosphino-imidazolium salts on the structures of Ir-complexes and catalysis for hydroformylation. Journal of Molecular Catalysis A, 2016, 411, 337-343.	4.8	21
134	Efficient and recyclable Rh-catalytic system with involvement of phosphine-functionalized phosphonium-based ionic liquids for tandem hydroformylation–acetalization. Green Energy and Environment, 2017, 2, 419-427.	8.7	21
135	Integrating P2 into O′3 toward a robust Mn-Based layered cathode for sodium-ion batteries. Journal of Materials Chemistry A, 2020, 8, 23820-23826.	10.3	21
136	Impurity induced non-bulk stacking in chemically exfoliated h-BN nanosheets. Nanoscale, 2013, 5, 2290.	5.6	20
137	Magnetoelectricity coupled exchange bias in BaMnF4. Scientific Reports, 2015, 5, 18392.	3.3	20
138	Synthesis of CrOx/C catalysts for low temperature NH3-SCR with enhanced regeneration ability in the presence of SO2. RSC Advances, 2018, 8, 3858-3868.	3.6	20
139	Improved memory functions in multiferroic tunnel junctions with a dielectric/ferroelectric composite barrier. Applied Physics Letters, 2015, 107, .	3.3	19
140	Promotion effect of water on hydroformylation of styrene and its derivatives with presence of amphiphilic zwitterionic phosphines. Journal of Molecular Catalysis A, 2015, 407, 212-220.	4.8	19
141	Phosphonium-based aminophosphines as bifunctional ligands for sequential catalysis of one-pot hydroformylation–acetalization of olefins. Catalysis Science and Technology, 2016, 6, 3854-3861.	4.1	19
142	Improving the Electrochemical Properties of the Manganese-Based P3 Phase by Multiphasic Intergrowth. Inorganic Chemistry, 2018, 57, 15584-15591.	4.0	19
143	Bright-field scanning confocal electron microscopy using a double aberration-corrected transmission electron microscope. Ultramicroscopy, 2011, 111, 877-886.	1.9	18
144	Intrinsic ferromagnetism and quantum transport transition in individual Fe-doped Bi <sub>2</sub> Se <sub>3</sub> topological insulator nanowires. Nanoscale, 2017, 9, 12372-12378.	5.6	18

#	Article	IF	CITATIONS
145	Effect of Sodium Content on the Electrochemical Performance of Li-Substituted, Manganese-Based, Sodium-Ion Layered Oxide Cathodes. ACS Applied Materials & Interfaces, 2020, 12, 2191-2198.	8.0	18
146	Fast deterministic single-exposure coherent diffractive imaging at sub-Ångström resolution. Physical Review B, 2013, 87, .	3.2	17
147	Electron energy loss spectroscopy of nano-scale CrAlYN/CrN–CrAlY(O)N/Cr(O)N multilayer coatings deposited by unbalanced magnetron sputtering. Thin Solid Films, 2010, 518, 5121-5127.	1.8	16
148	Voltage polarity manipulation of the magnetoresistance sign in organic spin valve devices. Applied Physics Letters, 2014, 104, 262402.	3.3	16
149	Tuning carrier mobility without spin transport degrading in copper-phthalocyanine. Applied Physics Letters, 2015, 107, .	3.3	16
150	Four-state non-volatile memory in a multiferroic spin filter tunnel junction. Applied Physics Letters, 2016, 109, .	3.3	16
151	Effect of nitrogen-doped PtRu/graphene catalyst on its activity and durability for methanol oxidation. Journal of Applied Electrochemistry, 2016, 46, 895-900.	2.9	16
152	Single-Atom Tailoring of Two-Dimensional Atomic Crystals Enables Highly Efficient Detection and Pattern Recognition of Chemical Vapors. ACS Sensors, 2022, 7, 1533-1543.	7.8	16
153	Towards Sub-Angström Ptychographic Diffractive Imaging. Microscopy and Microanalysis, 2013, 19, 706-707.	0.4	15
154	Core–shell–shell heterostructures of α-NaLuF <sub>4</sub> :Yb/Er@NaLuF <sub>4</sub> :Yb@MF <sub>2</sub> (M = Ca, Sr, Ba) with remarkably enhanced upconversion luminescence. Dalton Transactions, 2016, 45, 11129-11136.	3.3	15
155	Three-dimensional elemental mapping of hollow Fe2O3@SiO2 mesoporous spheres using scanning confocal electron microscopy. Applied Physics Letters, 2012, 100, .	3.3	14
156	Ferroelectric Polarization-Modulated Interfacial Fine Structures Involving Two-Dimensional Electron Gases in Pb(Zr,Ti)O <sub>3</sub> /LaAlO <sub>3</sub> /SrTiO <sub>3</sub> Heterostructures. ACS Applied Materials & Interfaces, 2018, 10, 1374-1382.	8.0	14
157	Preparation and characterization of a flexible ferroelectric tunnel junction. Applied Physics Letters, 2020, 116, .	3.3	14
158	Monodispersed Pt3Ni Nanoparticles as a Highly Efficient Electrocatalyst for PEMFCs. Catalysts, 2019, 9, 588.	3.5	13
159	Thicknessâ€Dependent Asymmetric Potential Landscape and Polarization Relaxation in Ferroelectric Hf <i><sub>x</sub></i> Zr <sub>1â^'</sub> <i><sub>x</sub></i> O <sub>2</sub> Thin Films through Interfacial Bound Charges. Advanced Electronic Materials, 2019, 5, 1900554.	5.1	13
160	Superior-capacity binder-free anode electrode for lithium-ion batteries: Co <sub>x</sub> Mn <sub>y</sub> Ni <sub>z</sub> O nanosheets with metal/oxygen vacancies directly formed on Cu foil. Nanoscale, 2019, 11, 5080-5093.	5.6	13
161	Insight into the Structural Disorder in Honeycomb-Ordered Sodium-Layered Oxide Cathodes. IScience, 2020, 23, 100898.	4.1	13
162	High-Performance CVD MoS <sub>2</sub> Transistors with Self-Aligned Top-Gate and Bi Contact. , 2021,		13

**,** •

#	Article	IF	CITATIONS
163	Three-dimensional analysis of nanoparticles on carbon support using aberration-corrected scanning confocal electron microscopy. Applied Physics Letters, 2012, 101, .	3.3	12
164	Immobilization of a rhodium catalyst using a diphosphine-functionalized ionic liquid in RTIL for the efficient and recyclable biphasic hydroformylation of 1-octene. Faraday Discussions, 2016, 190, 219-230.	3.2	12
165	Revealing chemical processes and kinetics of drug action within single living cells via plasmonic Raman probes. Scientific Reports, 2017, 7, 2296.	3.3	12
166	Mott insulator to metal transition driven by oxygen incorporation in epitaxial LaTiO3 films. Applied Physics Letters, 2019, 115, .	3.3	12
167	Image Contrast in Aberration-Corrected Scanning Confocal Electron Microscopy. Advances in Imaging and Electron Physics, 2010, 162, 45-76.	0.2	11
168	Vertically Grown Fewâ€Layer MoS <sub>2</sub> Nanosheets on Hierarchical Carbon Nanocages for Pseudocapacitive Lithium Storage with Ultrahighâ€Rate Capability and Longâ€Term Recyclability. Chemistry - A European Journal, 2019, 25, 3843-3848.	3.3	11
169	A P2@Tunnel Heterostructure Cathode for Highâ€Performance Sodiumâ€ion Batteries. ChemElectroChem, 2020, 7, 4383-4389.	3.4	11
170	Intercalation and hybrid heterostructure integration of two-dimensional atomic crystals with functional organic semiconductor molecules. Nano Research, 2020, 13, 2917-2924.	10.4	11
171	Metastable γ-CsPbI <sub>3</sub> Perovskite Nanocrystals Created Using Aged Orthorhombic CsPbBr <sub>3</sub> . Journal of Physical Chemistry C, 2021, 125, 7109-7118.	3.1	11
172	Contrast in atomically resolved EF-SCEM imaging. Ultramicroscopy, 2013, 134, 185-192.	1.9	10
173	Atomically Resolved Scanning Confocal Electron Microscopy Using a Double Aberration-corrected Transmission Electron Microscope. Microscopy and Microanalysis, 2014, 20, 376-377.	0.4	10
174	Influence of electrostatic repulsive force and electron-withdrawing effect in ionic diphosphine on regioselectivity of rhodium-catalyzed hydroformylation of 1-octene. Journal of Molecular Catalysis A, 2015, 402, 37-45.	4.8	10
175	Off-stoichiometric Li3-3V2+(PO4)3/C as cathode materials for high-performance lithium-ion batteries. Journal of Power Sources, 2015, 293, 922-928.	7.8	10
176	High-resolution characterization of multiferroic heterojunction using aberration-corrected scanning transmission electron microscopy. Applied Physics Letters, 2017, 110, .	3.3	10
177	Precipitate formations with self-adaptive elemental diffusion and segregation in T92 steel. Journal of Alloys and Compounds, 2017, 693, 264-278.	5.5	10
178	Gramâ€Scale Synthesized Twoâ€Dimensional VSe <sub>2</sub> and SnSe <sub>2</sub> for Ultrahigh Electrocatalytic Sulfion Recycling. Advanced Materials Interfaces, 2022, 9, .	3.7	10
179	Two-Stage Assembly of Nanoparticle Superlattices with Multiscale Organization. Nano Letters, 2022, 22, 3809-3817.	9.1	10
180	High spatial resolution imaging of the segregation of reactive elements to oxide grain boundaries in alumina scales. Materials at High Temperatures, 2009, 26, 293-298.	1.0	9

#	Article	IF	CITATIONS
181	A general approach to realizing perovskite nanocrystals with insulating metal sulfate shells. Nanoscale, 2021, 13, 10329-10334.	5.6	9
182	Patterning the two dimensional electron gas at the LaAlO3/SrTiO3 interface by structured Al capping. Applied Physics Letters, 2017, 110, .	3.3	8
183	Development of in situ optical–electrical MEMS platform for semiconductor characterization. Ultramicroscopy, 2018, 194, 57-63.	1.9	8
184	Experimental and theoretical studies of the ternary thiophosphate PbPS <sub>3</sub> featuring ethane-like [P <sub>2</sub> S <sub>6</sub> ] <sup>4â^'</sup> units. Dalton Transactions, 2020, 49, 17221-17229.	3.3	8
185	Non-invasive digital etching of van der Waals semiconductors. Nature Communications, 2022, 13, 1844.	12.8	8
186	Controllable Edge Epitaxy of Helical GeSe/GeS Heterostructures. Nano Letters, 2022, 22, 5086-5093.	9.1	8
187	Enhancement of tunneling electroresistance by interfacial cation intermixing in ferroelectric tunnel junctions. Applied Surface Science, 2020, 512, 145707.	6.1	7
188	Large-Area Freestanding Weyl Semimetal WTe2 Membranes. Chinese Physics Letters, 2021, 38, 017101.	3.3	7
189	A Transmission Electron Microscopy Study of CoFe2O4 Ferrite Nanoparticles in Silica Aerogel Matrix Using HREM and STEM Imaging and EDX Spectroscopy and EELS. Microscopy and Microanalysis, 2010, 16, 200-209.	0.4	6
190	Catalytic reduction of NOx by CO over a Ni–Ga based oxide catalyst. Journal of Materials Chemistry A, 2015, 3, 15133-15140.	10.3	6
191	Chemical strain-dependent two-dimensional transport at <mml:math xmlns:mml="http://www.w3.org/1998/Math/MathML"&gt; <mml:mrow> <mml:mi>R</mml:mi> <mml:msub> <mml:m interfaces <mml:math< td=""><td>text&gt;AlO<!--</td--><td>/mml:mtext</td></td></mml:math<></mml:m </mml:msub></mml:mrow></mml:math 	text>AlO </td <td>/mml:mtext</td>	/mml:mtext

#	Article	IF	CITATIONS
199	Low Dose Defocused Probe Electron Ptychography Using a Fast Direct Electron Detector. Microscopy and Microanalysis, 2018, 24, 186-187.	0.4	5
200	Reliability of Ultrathin High-Î $^{ m o}$ Dielectrics on Chemical-vapor Deposited 2D Semiconductors. , 2020, , .		5
201	Scanning Transmission Electron Microscopy Study of the Evolution of Needle-Like Nanostructures in CoFe2O4and NiFe2O4Silica Nanocomposite Aerogels. Journal of Physical Chemistry C, 2011, 115, 5358-5365.	3.1	4
202	FABRICATION OF LATERAL ORGANIC SPIN VALVES BASED ON La0.7Sr0.3MnO3 ELECTRODES. Spin, 2014, 04, 1440008.	1.3	4
203	Reactive molecular beam epitaxial growth and in situ photoemission spectroscopy study of iridate superlattices. AIP Advances, 2017, 7, .	1.3	4
204	Strain-driven lattice distortion and the resultant magnetic properties of La0.7Sr0.3MnO3/BaTiO3 superlattices. Applied Physics Letters, 2019, 115, 201604.	3.3	4
205	Understanding the role of aluminium in determining the surface structure and electrochemical performance of layered cathodes. Nanoscale, 2019, 11, 13007-13016.	5.6	4
206	Linear correlation between the c-axis lattice constant and superconducting critical temperature in FeSe0.5Te0.5 thin films. Materials Research Express, 2020, 7, 046002.	1.6	4
207	Microstructure and Dielectric Properties of Tungsten Bronze Structured KLN and BNN Ceramics: TiO2 Effect. International Journal of Modern Physics B, 2003, 17, 1267-1272.	2.0	3
208	Experimental setup for energy-filtered scanning confocal electron microscopy (EFSCEM) in a double aberration-corrected transmission electron microscope. Journal of Physics: Conference Series, 2010, 241, 012012.	0.4	3
209	Three-dimensional observation of SiO2 hollow spheres with a double-shell structure using aberration-corrected scanning confocal electron microscopy. Microscopy (Oxford, England), 2012, 61, 159-169.	1.5	3
210	Fast and Low-dose Electron Ptychography. Microscopy and Microanalysis, 2018, 24, 224-225.	0.4	3
211	An example of high- <i>T</i> , high-symmetry crystallization: Spherical (Mg,Fe)-oxides formed by particle attachment in the shocked martian meteorite Northwest Africa 7755. American Mineralogist, 2019, 104, 150-157.	1.9	3
212	A facile method for precise layer number identification of two-dimensional materials through optical images. Optics Communications, 2019, 440, 21-25.	2.1	3
213	Interface-Guided Formation of 2D Ultrathin MnO <sub>2</sub> Nanosheets with Abundant Oxygen Defects for High Performance Supercapacitors. ACS Applied Energy Materials, 2022, 5, 6962-6969.	5.1	3
214	Energy Filtered Scanning Confocal Electron Microscopy in a Double Aberration-Corrected Transmission Electron Microscope. Microscopy and Microanalysis, 2009, 15, 42-43.	0.4	2
215	Smart Acquisition EELS. Journal of Physics: Conference Series, 2010, 241, 012010.	0.4	2
216	Phasoid intergrowth between the double perovskite Sr2MgMoO6 and the n=2 R-P phase Sr3Mo2O7. Solid State Ionics, 2010, 181, 889-893.	2.7	2

#	Article	IF	CITATIONS
217	A perturbation theory study of electron vortices in electromagnetic fields: The case of infinitely long line charge and magnetic dipole. Micron, 2014, 63, 9-14.	2.2	2
218	Generalized Fourier Holography Meets Coherent Diffractive Imaging. Microscopy Today, 2015, 23, 28-33.	0.3	2
219	3D Electron Ptychography. Microscopy and Microanalysis, 2019, 25, 1802-1803.	0.4	2
220	Three Dimensional Characterization of a Silica Hollow Sphere with an Iron Oxide Core by Annular Dark Field Scanning Confocal Electron Microscopy. Microscopy and Microanalysis, 2010, 16, 1836-1837.	0.4	1
221	Three-Dimensional Resolution Limits and Image Contrast Mechanisms in Scanning Confocal Electron Microscopy. Microscopy and Microanalysis, 2010, 16, 1834-1835.	0.4	1
222	Chromatic Confocal Electron Microscopy with a Finite Pinhole Size. Journal of Physics: Conference Series, 2012, 371, 012002.	0.4	1
223	Current Developments of Scanning Confocal Electron Microscopy in a Double Aberration-Corrected Transmission Electron Microscope. Microscopy and Microanalysis, 2012, 18, 532-533.	0.4	1
224	Multislice Simulation of Dynamical Elastic Scattering and Orbital Angular Momentum of Vortex Beams in Crystals. Microscopy and Microanalysis, 2013, 19, 1184-1185.	0.4	1
225	Structural and chemical characterization of novel NixZn1â^'xGa2O4 nanocatalysts at atomic resolution. Applied Surface Science, 2015, 353, 419-424.	6.1	1
226	Electron ptychography using an ultrafast direct electron detector. Microscopy and Microanalysis, 2019, 25, 20-21.	0.4	1
227	Anomalous Linear Layer-Dependent Blue Shift of Ultraviolet-Range Interband Transition in Two-Dimensional MoS <sub>2</sub> . Journal of Physical Chemistry C, 2020, 124, 1609-1616.	3.1	1
228	Ptychographic Single Particle Analysis for Biological Science. Microscopy and Microanalysis, 2021, 27, 190-192.	0.4	1
229	Atomic-resolution study of charge transfer effects at the <mmi:math xmlns:mml="http://www.w3.org/1998/Math/MathML"&gt;<mml:mrow><mml:mi>LaTi</mml:mi><mml:msub><mml: mathvariant="normal"&gt;O<mml:mn>3</mml:mn></mml: </mml:msub></mml:mrow><mml:mo>/</mml:mo><r mathvariant="normal"&gt;O<mml:mn>3</mml:mn></r </mmi:math 	mi nn <b>sl.2</b> nrow	> amml:mi>t
230	High Angle Annular Dark Field Imaging On and Away from the Pole. Microscopy and Microanalysis, 2005, 11, .	0.4	0
231	Establishment of Annular Dark-Field Scanning Confocal Electron Microscopy using a Double Aberration-Corrected Microscope. Microscopy and Microanalysis, 2010, 16, 1888-1889.	0.4	0
232	Three-Dimensional Crystal Structure Mapping by Diffractive Scanning Confocal Electron Microscopy (SCEM). Journal of Physics: Conference Series, 2012, 371, 012003.	0.4	0
233	Nanohalos: A manifestation of electron channelling in gold nanoparticles. Ultramicroscopy, 2012, 120, 10-15.	1.9	0
234	Imaging and diffraction characterisation of 2D inorganic nanostructures. Journal of Physics: Conference Series, 2012, 371, 012071.	0.4	0

#	Article	IF	CITATIONS
235	Electron Ptychography: From 2D to 3D Reconstructions. Microscopy and Microanalysis, 2017, 23, 346-347.	0.4	0
236	Interface electron transfer and thickness dependent transport characteristics of La <sub>0.7</sub> Sr <sub>0.3</sub> VO <sub>3</sub> thin films. Journal of Physics Condensed Matter, 2019, 31, 245002.	1.8	0
237	Developing Multifunctional and High Resolution In-situ TEM Holders. Microscopy and Microanalysis, 2019, 25, 1854-1855.	0.4	0
238	Low Dose Electron Ptychography for Cryo-biological Imaging. Microscopy and Microanalysis, 2020, 26, 1488-1490.	0.4	0
239	Reliability of Ultrathin High \$-mathcal{K}\$ Dielectrics on 2D Semiconductors. , 2021, , .		0
240	Characterizing soil mechanical response induced by drought climate using a novel micropenetrometer. , 2015, , 217-222.		0
241	Investigating the volume change characteristics of bentonite/sand mixture under hydro-mechanical coupling condition. , 2015, , 223-228.		0
242	Effect of grain size on soil moisture evaporation process. , 2015, , 451-454.		0
243	Aberration corrected STEM and EELS: Atomic scale chemical mapping. , 2008, , 1-2.		Ο